Solid–State Supercapacitors Based on Polyoxometalates–Based Crystalline Materials Modified with Polyaniline

Chen Wang[a], Zhi-Xin Gao[b], Hong-Ying Zang[*b], Tao-Wen Dong[*c], Zhong-Min Su[*ad]

[a] State Key Laboratory of Supramolecular Structure and Materials, Institute of Theoretical Chemistry，College of Chemistry, Jilin University, Changchun 130021, P. R. China

[b] Key Laboratory of Polyoxometalate and Reticular Material Chemistry of Ministry of Education at Universities of Jilin Province, Faculty of Chemistry, Northeast Normal University, Changchun 130024, P. R. China

[c] State Key Laboratory of Automotive Simulation and Control, and School of Materials Science & Engineering, Jilin University, Changchun 130012, China

[d] School of Chemistry and Environmental Engineering, Changchun University of Science and Technology, Changchun 130022, P. R. China; Jilin Provincial Science and Technology Innovation Center of Optical Materials and Chemistry, Changchun 130022, P. R. China; Joint Sino-Russian Laboratory of Optical Materials and Chemistry, Changchun 130022, P. R. China

Materials and General Methods

The FT-IR spectra were taken on a Varian FT-IR 640 spectrometer (KBr pellets) in the range of 400-4000 cm^{-1}. Powder X-ray diffraction (PXRD) patterns were recorded on an Ultima IV with D/teX Ultra diffractometer at 40 kV, 40 mA with Cu Kα ($\lambda = 1.5406$ Å) radiation in the 2θ range of 5–50°. The morphology of electrodes and complexes were analyzed by scanning electron microscopy (SEM, Hitachi SU-70). XPS measurement was carried out on VG ESCALAB MKII, Al-Kα radiation. A CHI760 electrochemical workstation was used to measure electrochemical capability and collect data. The classical three-electrode system was adopted, in which the saturated calomel electrode (SCE) was used as reference electrode and the Pt wire as the counter electrode.

Preparation of complexs 1–2

Synthesis of Complex **1** $H_2\{Co_2Py_4(H_2O)_4[Co_2\{Co[Mo_6O_{12}(OH)_3(HPO_4)(PO_4)_3]_2\}]\}\cdot4DMF\cdot10H_2O$ (**1**)

CoCO$_3$ (0.164 g, 1.38 mmol), Na$_2$MoO$_4$ (0.253 g, 1.23 mmol), 1 mL concentrated H$_3$PO$_4$ and 1 mL pyridine were dissolved in 5 mL deionized water and 1 mL DMF at room temperature. The suspension was stirred for 30 min in air. The resulting suspension was sealed in a Teflon-lined autoclave (25 mL) and kept at 150 °C for 3 days. After cooling to room temperature, red block crystals of **1** (0.271 g, yield 48% based on Mo) were obtained. Anal. Calcd for **1** C$_{32}$H$_{84}$Co$_5$N$_8$O$_{80}$P$_8$Mo$_{12}$ (3554) : C 10.81, P 6.97, N 3.15 %. Found: C 10.79, P 7.02, N 3.12 %.

Synthesis of Complex **2** $H_6Py_2[Mn_2\{Mn[Mo_6O_{12}(OH)_3(HPO_4)_4]_2\}]\cdot6DMF\cdot4H_2O$ (**2**)

MnCl$_2$ (0.170 g, 1.35 mmol), Na$_2$MoO$_4$ (0.230 g, 1.11 mmol), 1 mL concentrated H$_3$PO$_4$ and 0.5 mL pyridine were dissolved in 5 mL deionized water and 1 mL DMF at room temperature. The suspension was stirred for 30 min in air. The resulting suspension was sealed in a Teflon-lined autoclave (25 mL) and kept at 160 °C for 3 days. After cooling to room temperature, orange-red block crystals of **2** (0.127 g, yield 28% based on Mo) were obtained. Anal. Calcd for **2** C$_{28}$H$_{72}$Mn$_3$N$_8$O$_{72}$P$_8$Mo$_{12}$ (3236) :

C 10.39, P 7.66, N 3.46 %. Found: C 10.41, P 7.71, N 3.50 %.

Preparation of working electrodes of complexes

The complexes, Ketjen black and PVDF (polyvinylidene fluoride) were mixed in a certain mass ratio (1: 1: 1), and then N-methylpyrrolidone was added to form a paste. The paste was ground about 5 mins, which was coated on the surface of carbon paper ($1\times1cm^2$), The electrode was dried at 60°C overnight. Finally, the mass loading of the materials is 3 mg.

Preparation of n@PANI–x electrodes

The electrochemical deposition method was used to prepare **n** @PANI–x electrodes. The detailed experimental steps are as follows [S1]: the as-preparing complexes electrodes were acted as working electrode in a three-electrodes system (saturated calomel electrode as reference and Pt wire as counter). The electrolyte was prepared by mixing 50 mL water, 1.2 mL aniline and 2.1 mL concentrated HCl. The electro-deposition experiments were conducted during a potential window between -0.2 – +1.0 V for different cycles, then the samples were dries at 60°C for 12h. According to different cycle numbers for coating PANI on complexes, the final electrode composites named **1**@PANI-1 (1 cycle), **1**@PANI-2 (2 cycles), **2**@PANI-1 (1 cycle) and **2**@PANI-2 (2 cycles).
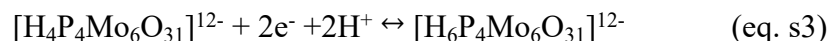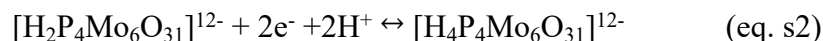
Preparation of H$_2$SO$_4$–gel electrolytes

2 g of 5wt% PVA aqueous solution, 0.1 g of glycerin (plasticzer) and 0.4 g concentrated H$_2$SO$_4$ soluiton, 2 μL of 25wt% glutaraldehyde (cross-linking agent) were mixed, stirring 12 h at room temperature to obtain a homogeneous solution.

Preparation of symmertrical supercapacitor

The newly prepared H$_2$SO$_4$–gel electroltyes was dropped on two **n**@PANI–1 electrodes, which was dried at room temperature. And then, two **n**@PANI–1 electrodes were affixed together and hot–pressed at 50 °C for 10 mins. The formed devices were places in a closed container with saturated potassium sulfate about 3 hours

The three pairs peaks (Figure 3a,b) are attributed to the redox processes of the Mo^V center of $[P_4Mo_6O_{31}]^{12-}$ polyanion, the possible redox reaction are as follow [S2]:

$$[P_4Mo_6O_{31}]^{12-} + 2e^- + 2H^+ \leftrightarrow [H_2P_4Mo_6O_{31}]^{12-} \qquad \text{(eq. s1)}$$

$$[H_2P_4Mo_6O_{31}]^{12-} + 2e^- + 2H^+ \leftrightarrow [H_4P_4Mo_6O_{31}]^{12-} \qquad \text{(eq. s2)}$$

$$[H_4P_4Mo_6O_{31}]^{12-} + 2e^- + 2H^+ \leftrightarrow [H_6P_4Mo_6O_{31}]^{12-} \qquad \text{(eq. s3)}$$

The specific capacity value, areal capacitance, energy density and corresponding power density can be calculated from the equations [S3]:

$$\text{Specific capacity} = \frac{2I \times \triangle t}{s \times \triangle V} \qquad \text{(eq. s4)}$$

$$\text{Areal capacitance} = \frac{2I \times \triangle t}{s \times \triangle V} \qquad \text{(eq. s5)}$$

$$\text{Energy density} = CV^2/2 \qquad \text{(eq. s6)}$$

$$\text{Power density} = 3600E/t \qquad \text{(eq. s7)}$$

Where I (A) is discharge current, ΔV (V) is potential change, m (g) is the amount of active material, s (cm^{-2}) is the area of electroactive, Δt (s) is discharge time, E (Wh/kg or Wh/g) is energy density, P (W/kg or W/g) is power density.

X-Ray crystallography study

A Bruker SMART APEX II with Mo-$K\alpha$ radiation ($\lambda = 0.71073$ Å) was used to collect X-Ray diffraction analyses data by using ω and θ scan mode at 293 K. The detailed crystal data and structure refinement for **1**–**2** is shown in Table S1. Selected bond lengths and angles are listed in Table S2. Crystallographic data for the compounds reported in this work have been deposited in the Cambridge Crystallographic Data Center with CCDC numbers 2204878-2204879 for **1**–**2**.
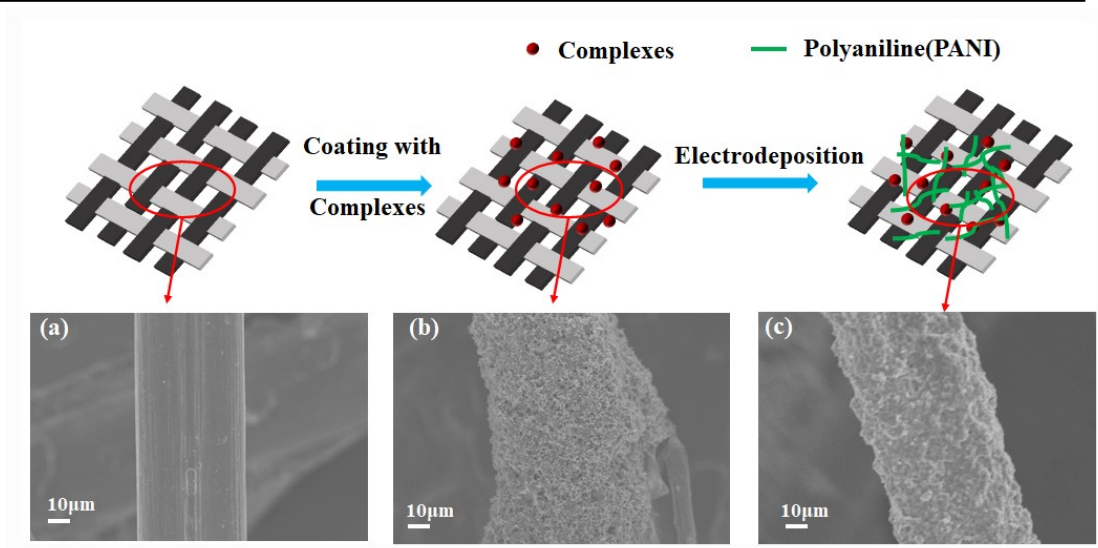
Figure S1. Schematic diagram of the two–step fabrication of **n@** PANI– x electrodes. (a) the carbon paper, (b) after coating with complexes, (c) after electrodeposition of aniline.
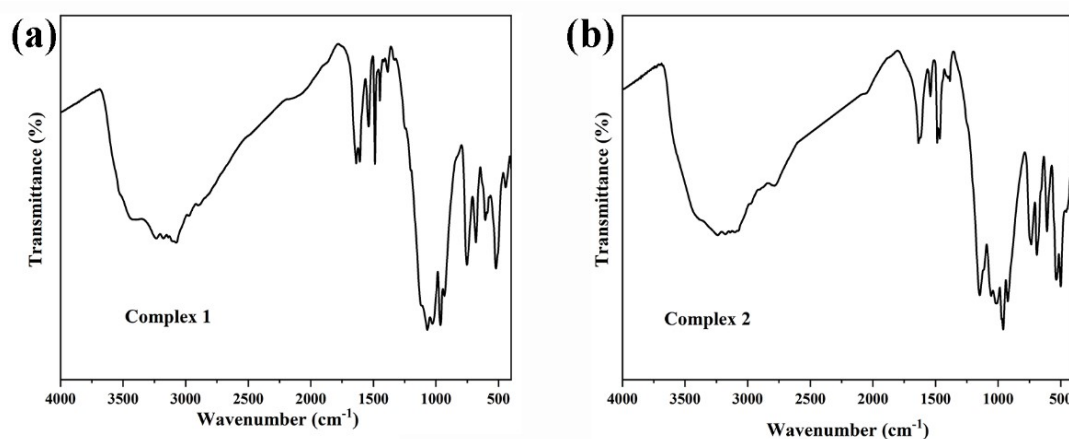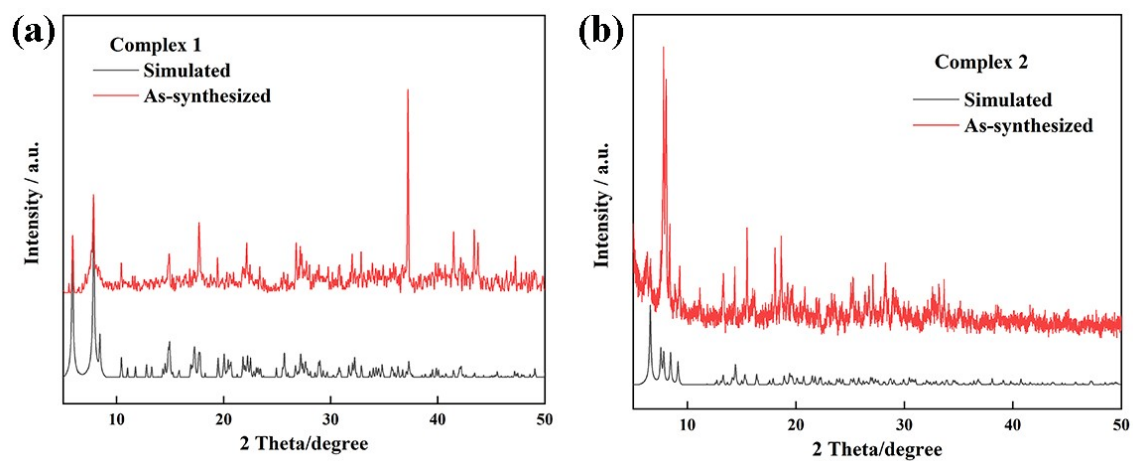

Figure S2. The IR spectrum of complexes **1**–**2.**

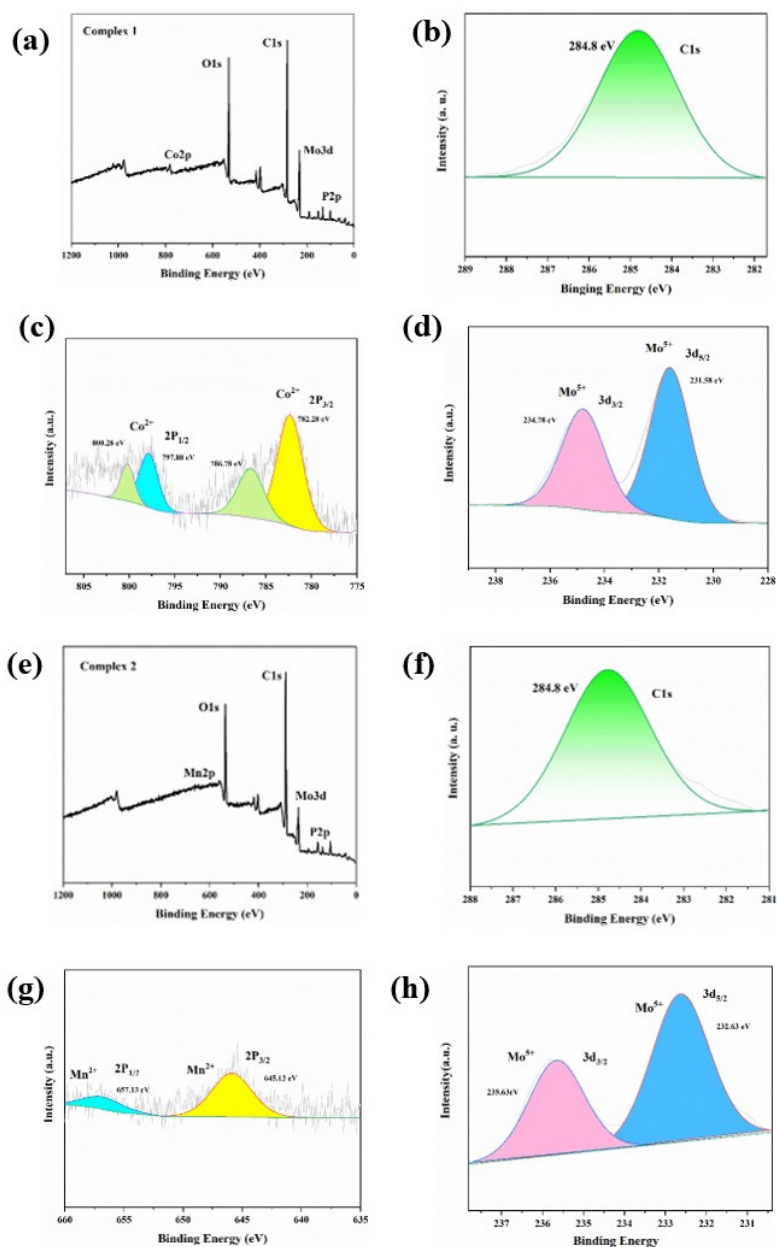Figure S3. Power X-ray diffraction patterns of complexes **1**–**2**.

Figure S4. The X-Ray photoelectron spectroscopy of complexes **1**–**2** (a, e); The XPS high-resolution for C(1s) Mo(3d), Co(2P) and Mn(2P) for complexes **1**–**2**.
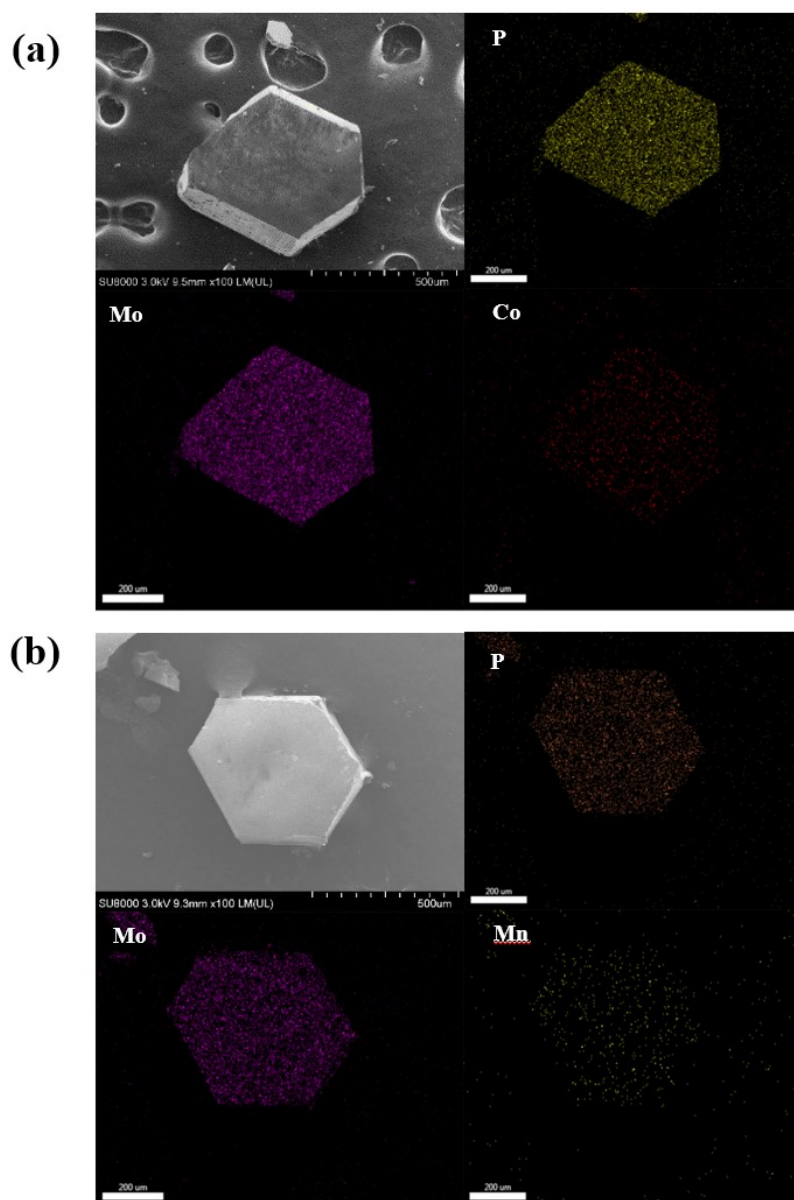
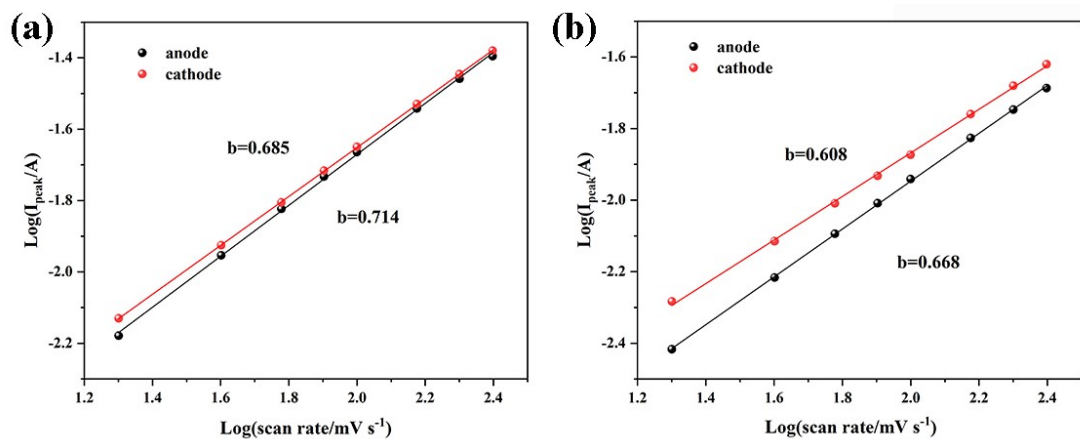Figure S5. The SEM and EDS mapping of complexes **1**–**2.**

Figure S6. (a-b) The relationship between peak currents and scan rates to determine *b* value.

Figure S7. (a-b) The cyclic voltammograms of **1**@PANI–1, **1**@PANI–2 in 0.5M H$_2$SO$_4$ solution at different scan rates (fr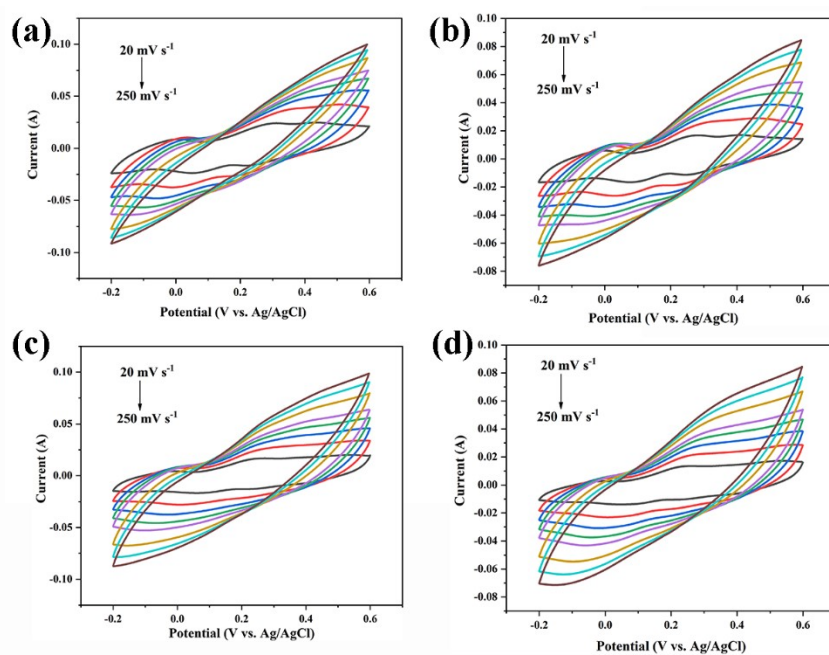om inner to outer: 20, 40, 60, 80, 100, 150, 200, 250 mV s^{-1}). (c-d) The cyclic voltammograms of **2**@PANI–1, **2**@PANI–2 in 0.5M H$_2$SO$_4$ solution at different scan rates (from inner to outer: 20, 40, 60, 80, 100, 150, 200, 250 mV s^{-1}).
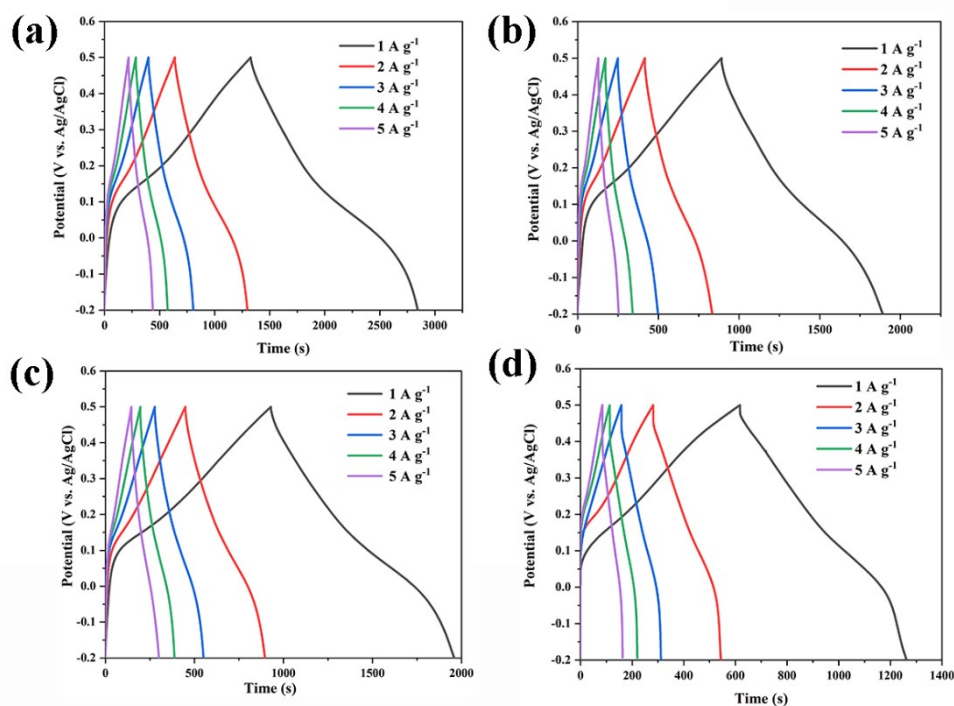
Figure S8. The GCD curves of **1**@PANI–1(a), **1**@PANI–2(b), **2**@PANI–1(c), **2**@PANI–2(d) from 1 A g^{-1} to 5 A g^{-1}.
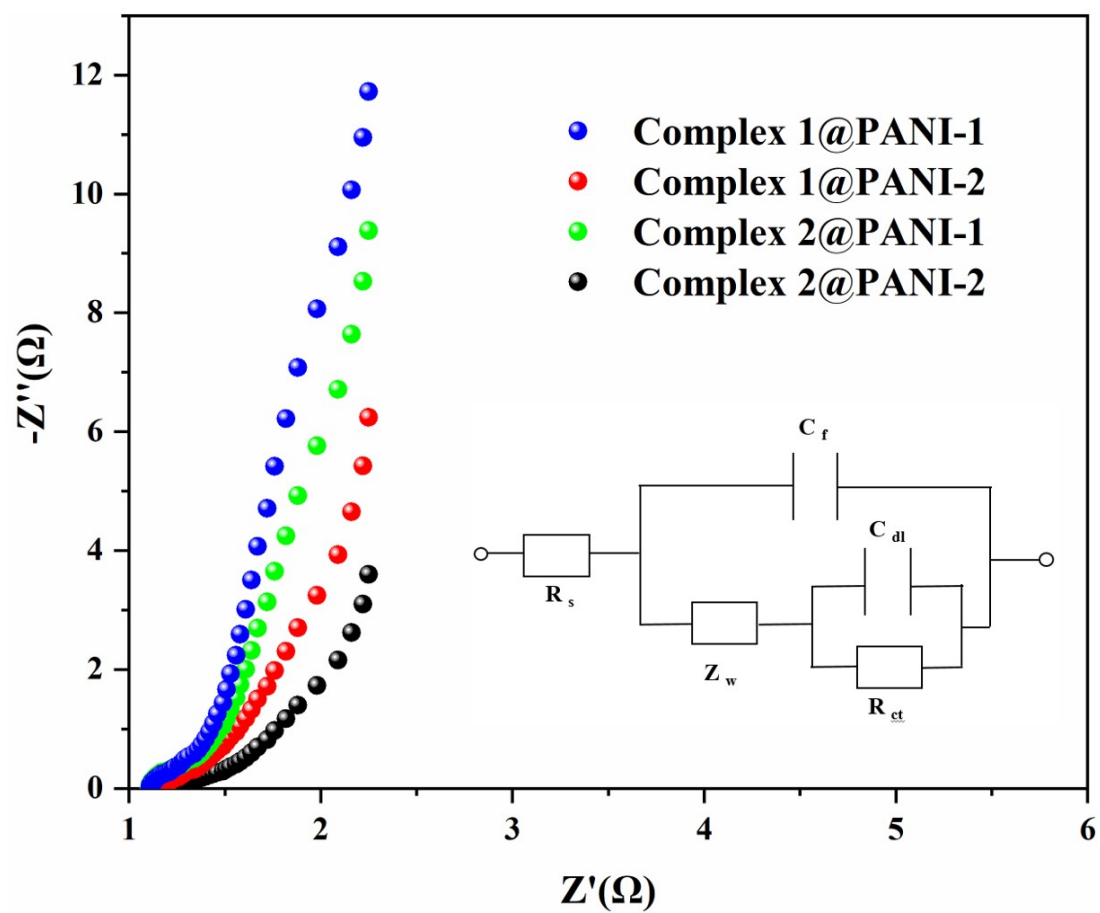
Figure S9. The EIS spectra of **n**@PANI−x.

The mechanism of Conductive Polymers can be divided in two types: p-doping upon

oxidization and n-doping upon reduction, and the doping/dedoping process of PANI

can show as follow [S4, S5]:

$$CP \rightarrow CP^{n+}(A^-)_n + ne^- \text{ (p-doping)} \qquad \text{(eq. s4)}$$
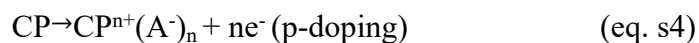
Where A- represents the anion in the electrolyte.
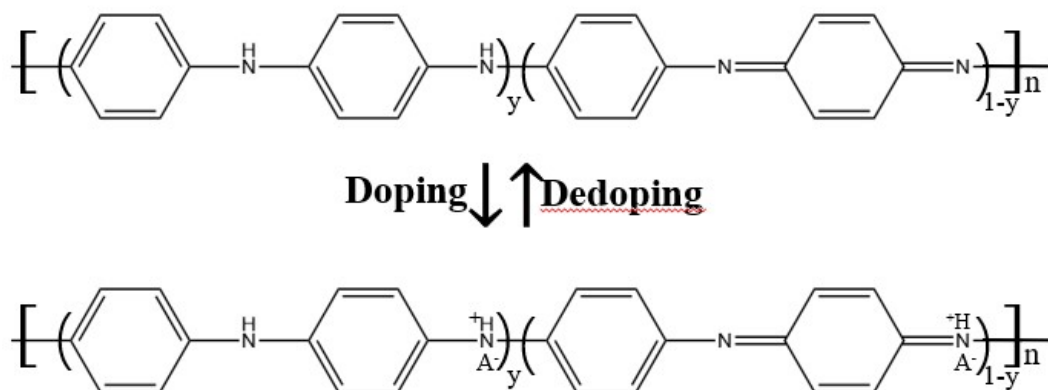
Figure S10. The mechanism of doping/dedoping process of PANI
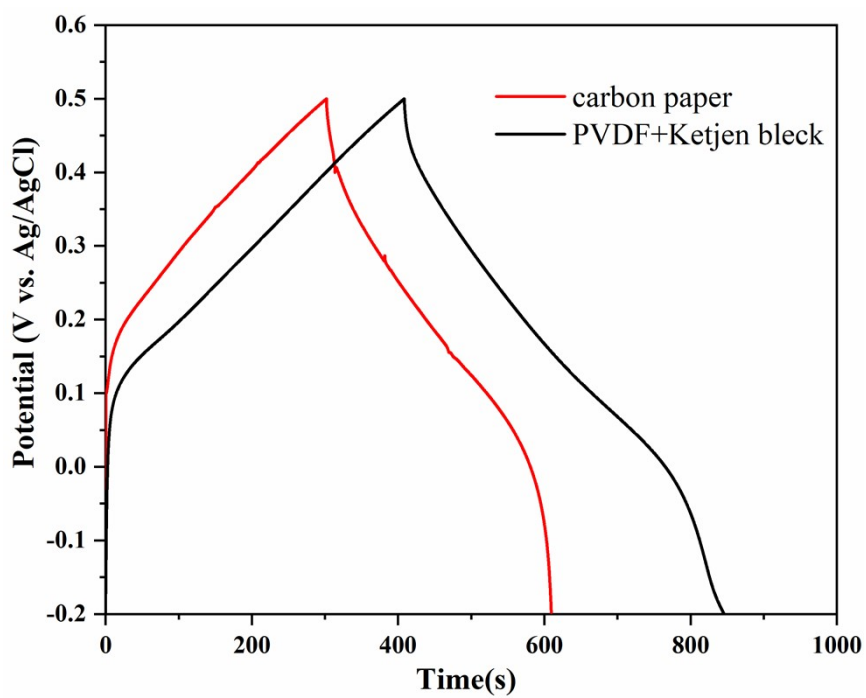
Figure S11. The GCD curves of carbon paper and PVDF + Ketjen black at the current density of 1 A g^{-1}.
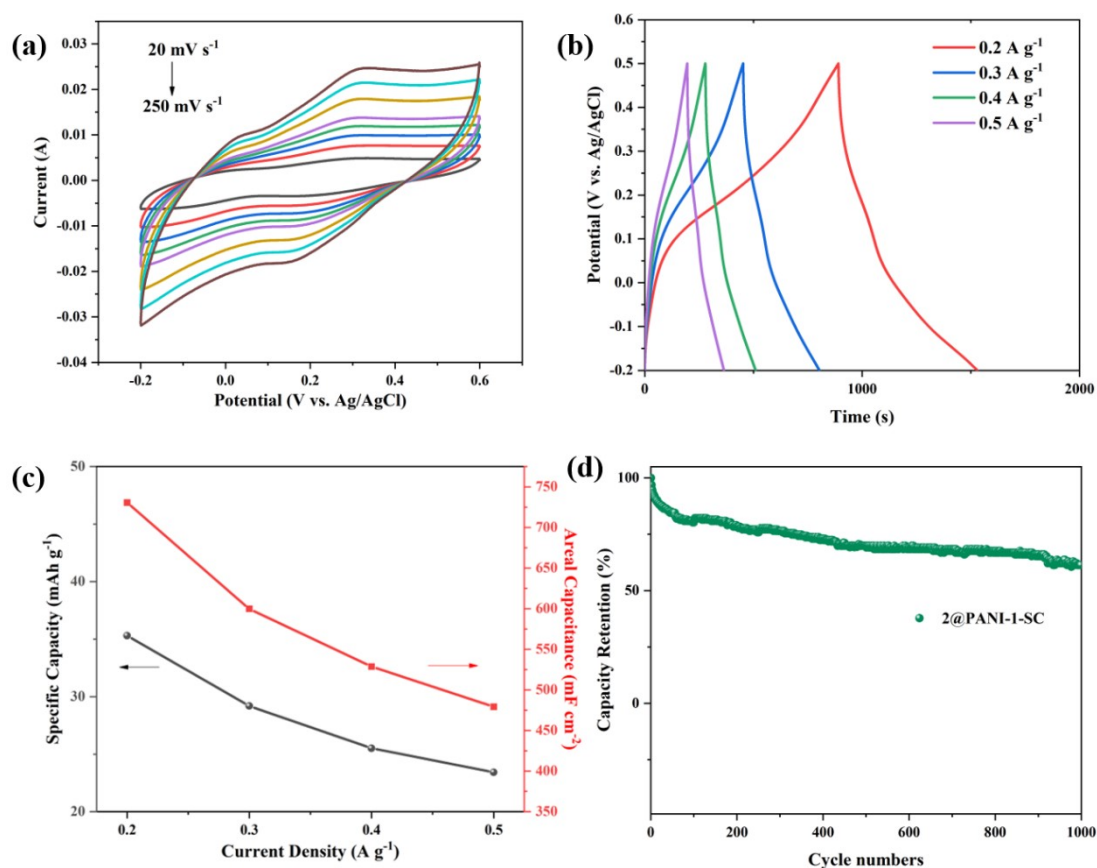
Figure S12. (a) CV curves of **2**@PANI−1−SC device at different scan rates from 20 mV s^{-1} to 250 mV s^{-1}. (b) GCD curves of **2**@PANI−1−SC device at different current densities from 0.2 A g^{-1} to 0.5 A g^{-1}. (c) Variation of C_s and C_a of **2**@PANI−1−SC device as a function of the current density. (d) capacitance retention of **2**@PANI−1−SC device after 1000 cycles at 0.5 A g^{-1}.
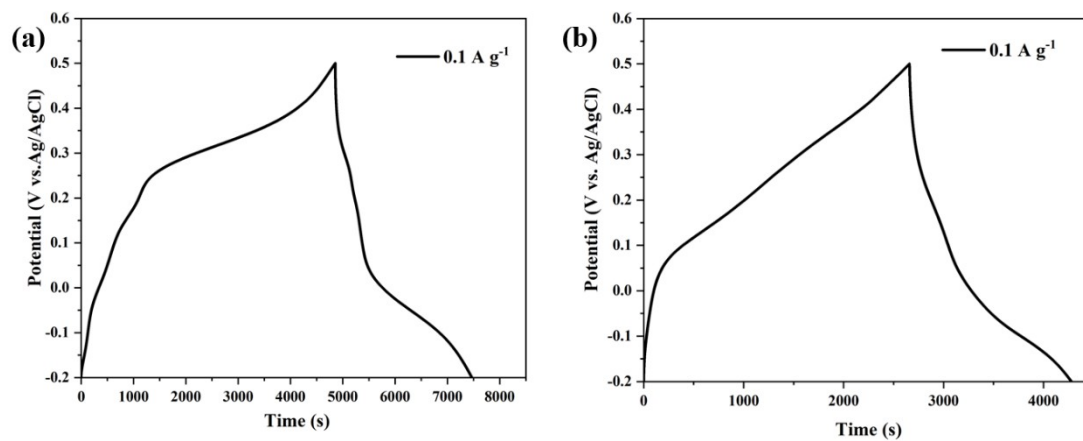
Figure S13. (a) GCD curves of **1**@PANI−1−SC device at current density of 0.1A g^{-1}. (b) GCD curves of **2**@PANI−1−SC device at current density of 0.1A g^{-1}.

Table. S1. Crystal Data and Structure Refinement for Complexes **1–2**.

	1	2
formula	$C_{20}H_{84}Co_5N_4O_{80}$	$C_{28}H_{72}Mn_3N_8O_{72}$
	P_8Mo_{12}	P_8Mo_{12}
Fw	3554.76	3236.79
crystal system	Monoclinic	Triclinic
space group	$C/2m$	$P–1$
a (Å)	24.257(2)	13.3857(10)
b (Å)	13.3272(10)	13.8827(9)
c (Å)	17.421(3)	15.0491(12)
α (°)	90	112.172 (3)
β (°)	120.353(2)	94.810(4)
γ (°)	90	118.441(3)
V (Å^3)	4859.9(10)	2154.6(3)
Z	2	1
D_c (g·cm^{-3})	2.429	2.495
μ (mm^{-1})	2.572	2.376
$F(000)$	3462	1571
R_1[a] [I > 2σ(I)]	0.0413	0.0374
wR_2[b] (all data)	0.1135	0.1023
GOF on F^2	1.063	1.033

[a]$R_1 = \sum||F_0| - |F_C||/\sum|F_0|$; [b]$wR_2 = \sum[w(F_0^2–F_C^2)^2]/\sum[w(F_0^2)^2]^{1/2}$

Table. S2. Selected bond distances(Å) and angles (°) for Complexes **1**–**2**.

Complex **1**			
Co(1)–N(1)	2.214(6)	Co(1)–O(19)	2.120(3)
Co(1)–O1W	2.178(5)	Co(2)–O(18)	1.933(5)
Co(2)–O(17)	1.926(6)	Co(3)–O(12)	2.140(3)
Co(2)–O(3)	1.962(5)	Co(3)–O(9)	2.166(5)
Mo(3)–Mo(2)	2.5814(7)	Mo(2)–O(11)	1.669(5)
Mo(2)–O(12)	1.975(3)	Mo(2)–O(13)	1.937(4)
Mo(1)–O(2)	2.302(3)	Mo(1)–O(6)	2.061(5)
Mo(1)–O(7)	1.939(4)	Mo(1)–O(8)	1.677(4)
P(3)–O(16)	1.545(4)	P(3)–O(19)	1.528(5)
P(3)–O(17)	1.490(6)	P(1)–O(1)	1.553(15)
P(1)–O(2)	1.546(4)	P(1)–O(3)	1.516(3)
P(2)–O(6)	1.412(9)	P(2)–O(4)	1.440(9)
P(2)–O(5)	1.681(9)	N(1)–C(1)	1.330(9)
N(1)–C(5)	1.346(9)	C(2)–C(3)	1.371(13)
N(1)–Co(1)–O1W	89.4(2)	O(18)–Co(2)–O(3)	110.77(16)
O(19)–Co(1)–N(1)#5	92.2(2)	O(19)–Co(1)–O1W	175.60(18)
O(17)–Co(2)–O(18)	98.9(2)	O(12)–Co(3)–O(9)#2	84.37(13)
O(17)–Co(2)–O(3)	126.0(2)	O(12)–Co(3)–O(9)	95.62(13)
P(3)–O(16)–Mo(3)	135.4(2)	P(1)–O(1)–Mo(3)	126.71(12)
O(3)–P(1)–O(2)	111.90(19)	O(8)–Mo(1)–O(9)	103.1(2)
O(7)–Mo(1)–O(2)	82.98(19)	C(5)–N(1)–Co(1)	122.1(5)

Symmetry codes**:** #2 -1+X, +Y, +Z; #5 1-X, +Y, -Z

Complex **2**			
Mn(1)–O(3)	2.203(4)	Mn(1)–O(7)#5	2.198(3)
Mn(1)–O(3)#5	2.203(4)	Mn(1)–O(29)#2	2.194(3)
Mn(2)–O(22)	1.965(4)	Mn(2)–O(13)	1.952(4)
Mn(2)–O(14)	1.79(5)	Mn(2)–O(18)	1.948(4)

P(1)–O(17)	1.533(4)	P(1)–O(15)	1.540(4)
P(2)–O(5)	1.529(5)	P(2)–O(12)	1.573(5)
Mo(1)–O(3)	1.970(4)	Mo(1)–O(1)	1.677(4)
Mo(1)–O(2)	1.936(4)	Mo(2)–O(3)	1.963(3)
Mo(2)–O(2)	1.941(4)	Mo(2)–O(4)	1.678(4)
Mo(2)–O(5)	2.058(4)	Mo(2)–O(6)	2.095(4)
Mo(3)–O(6)	2.112(4)	Mo(3)–O(7)	1.968(3)
Mo(3)–O(8)	1.938(4)	Mo(3)–O(9)	1.677(4)
Mo(3)–O(11)	2.053(4)	Mo(4)–O(7)	1.975(4)
Mo(4)–O(8)	1.936(4)	Mo(4)–O(10)	1.677(4)
O(29)#4–Mn(1)–O(7)	84.39(13)	O(29)#2–Mn(1)–O(3)	96.24(13)
O(7)–Mn(1)–O(3)	95.81(13)	O(29)#4–Mn(1)–O(3)	83.76(3)
O(14)–Mn(2)–O(13)	94.2(13)	O(14)–Mn(2)–O(18)	105.3(17)
O(13)–Mn(2)–O(22)	108.68(18)	O(18)–Mn(2)–O(22)	113.31(18)
O(29)–Mo(5)–O(27)	86.11(14)	O(28)–Mo(5)–O(27)	156.56(15)
O(26)–Mo(5)–O(27)	96.15(18)	O(29)–Mo(6)–O(30)	85.68(14)
O(28)–Mo(6)–O(30)	155.51(15)	O(31)–Mo(6)–O(30)	97.98(18)
O(9)–Mo(3)–O(7)	101.98(18)	O(9)–Mo(3)–O(11)	95.37(19)
O(9)–Mo(3)–O(6)	97.26(19)	O(9)–Mo(3)–O(11)	95.73(19)

Symmetry codes**:** #2 -1+X, +Y, +Z; #4 1-X, 2-Y, 1-Z; #5 -X, 2-Y, 1-Z

Table. S3. Comparison of capacitance retention with other solid-state SCs

Materials	Cycle number	Capacitance retention(%)	Ref.
$PMo_{10}V_2$-ILs@MIL-100	100	75	S6
$[Zn(itmb)_3(H_2O)(HPMo_{12}O_{40})]\cdot4H_2O$	500	92.7	S7
$TBA_3[PMo_{12}O_{40}]$	10	80.7	S8
$Na_3[AlMo_6O_{24}H_6]$	50	91.2	S9
$SWNTs/Py–SiW_{11}$	100	37	S10
NAM−EDAG	1100	54.4	S11
$Mo_6–$ SCN	100	85	S12
NENU-507	100	63.5	S13
$TBA-PMo_{11}V/CNTs$	100	28.2	S14
ZIF-67	2000	80	S15
$CNTs–SiW_{11}$	100	54.6	S16
$Na_7H_2[PV_{14}O_{42}]$	150	57.2	S17
$(NH_4)_6[NiMo_9O_{32}]$	50	87.6	S18
Mn-Anderson/SWNT	100	27.4	S19
$3D\ rGO@PANI/PW_{12}$	50	87	S20
NNU-11	200	56.7	S21
CuPW/SWNTs	170	71.8	S22
(Py-Anderson)-CNTs	100	35.1	S23
$PMo_{12}/PANI/MWNTs$	100	63.6	S24
1@PANI-1-SC	1000	72.46	**This work**
2@PANI-2-SC	1000	61.37	**This work**

References

S1. C. M. Zhu, Y. He, Y. J. Liu, N. Kazantseva, P. Saha, Q. L. Cheng, ZnO@MOF@PANI core-shell nanoarrays on carbon cloth for high-performance supercapacitor electrodes, *J. Energy Chem.,* 2019, **35**, 124.

S2. X. Xin, N. Hu, Y. Y. Ma, Y. L. Wang, L. Hou, H. Zhang, Z. G. Han, Polyoxometalate-based crystalline materials as a highly sensitive electrochemical sensor for detecting trace Cr(VI), *Dalton Trans.,* 2020, **49**, 4570.

S3. D. M. Cheng, B. Li, S. Sun, L. J. Zhu, Y. Li, X. L. Wu, H. Y. Zang, Proton-Conducting Polyoxometalates as Redox Electrolytes Synergistically Boosting the Performance of Self-Healing Solid-State Supercapacitors with Polyaniline, *CCS Chem,* 2020, **2**, 1649.

S4. Y. Q. Wang, Y. Ding, X. L. Guo, G. H. Yu, Conductive polymers for stretchable supercapacitors, *Nano Res.,* 2019, **12**, 1978.

S5. A. K. Cuentas-Gallegos, M. Lira-Cantú, N. Casañ-Pastor, P. Gómez-Romero, Nanocomposite Hybrid Molecular Materials for Application in Solid-State Electrochemical Supercapacitors., *Adv. Funct. Mater.,* 2005, **15**, 1125.

S6. M. Zhang, A. M. Zhang, X. X. Wang, Q. Huang, X. S. Zhu, X. L. Wang, L. Z. Dong, S. L. Wang, Y. Q. Lan, Encapsulating ionic liquids into POM-based MOFs to improve their conductivity for superior lithium storage, *J. Mater. Chem. A,* 2018, **6**, 8735.

S7. G. N. Wang, T. T. Chen, C. Gómez-García, F. Zhang, M. Y. Zhang, H. Y. Ma, H. J. Pang, X. M. Wang, L. C. Tan, A High-Capacity Negative Electrode for Asymmetric Supercapacitors Based on a PMo_{12} Coordination Polymer with Novel Water-Assisted Proton Channels, *Small,* **2020**, 2001626.

S8. H. Wang, S. Hamanaka, Y. Nishimoto, S. Irle, T. Yokoyama, H. Yoshikawa, K. Awaga, In Operando X-ray Absorption Fine Structure Studies of Polyoxometalate Molecular Cluster Batteries: Polyoxometalates as Electron Sponges, *J. Am. Chem. Soc.,* 2012, **134**, 4918.

S9. E. F. Ni, S. Uematsu, N. Sonoyama, Anderson type polyoxomolybdate as cathode material of lithium battery and its reaction mechanism, *J. Power Sour.,* 2014, **267**, 673.

S10. D. Ma, L. Y. Liang, W. Chen, H. M. Liu, Y. F. Song, Covalently Tethered Polyoxometalate–Pyrene Hybrids for Noncovalent Sidewall Functionalization of Single-Walled Carbon Nanotubes as High-Performance Anode Material, *Adv. Funct. Mater.,* 2013, **23**, 6100.

S11. J. J. Xie, Y. Zhang, Y. L. Han, C. L. Li, High-Capacity Molecular Scale Conversion Anode Enabled by Hybridizing Cluster-Type Framework of High Loading with Amino-Functionalized Graphene, *ACS Nano,* 2016, **10**, 5304.

S12. R. N. N. Khan, N. Mahmood, C. L. Lv, G. H. Sima, J. Zhang, J. Hao, Y. L. Hou, Y. G. Wei, Pristine organo-imido polyoxometalates as an anode for lithium ion batteries, *RSC Adv.,* 2014, **4**, 7374.

S13. Y. Y. Wang, M. Zhang, S. L. Wang, S. R. Zhang, W. Xie, J. S. Qin, Z. M. Su, Y. Q. Lan, Diamondoid-structured polymolybdate-based metal–organic frameworks as high-capacity anodes for lithium-ion batteries, *Chem. Commun.,* 2017, **53**, 5204.

S14. J. Hu, Y. C. Ji, W. Chen, C. Streb, Y. F. Song, ''Wiring'' redox-active polyoxometalates to carbon nanotubes using a sonication-driven periodic functionalization strategy, *Energy Environ. Sci.,* 2016, **9**, 1095.

S15. L. Wang, X. Feng, L. T. Ren, Q. H. Piao, J. Q. Zhong, Y. B. Wang, H. W. Li, Y. F. Chen, B. Wang, Flexible Solid-State Supercapacitor Based on a Metal−Organic Framework Interwoven by Electrochemically-Deposited PANI, *J. Am. Chem. Soc.,* 2015, **137**, 4920.

S16. W. Chen, L. J. Huang, J. Hu, T. F. Li, F. F. Jia, Y. F. Song, Connecting carbon nanotubes to polyoxometalate clusters for engineering high-performance anode materials, *Phys. Chem. Chem. Phys.,* 2014, **16**, 19668.

S17. S. C. Huang, C. C. Lin, C. W. Hu, Y. F. Liao, T. Y. Chen, H. Y. Chen,

Vanadium-based polyoxometalate as electron/ion sponge for lithium-ion storage, *J. Power Sour.,* 2019, 435, 226702.

S18.   E. F. Ni, S. Uematsu, T. Tsukada, N. Somoyama, Lithium intercalation into polyoxomolybdate $(NH_4)_6[NiMo_9O_{32}]$ as the cathode material of lithium battery, *Solid State Ionics,* 2016, **285**, 83.

S19.   Y. C. Ji, J. Hu, L. J. Huang, W. Chen, C. Streb, Y. F. Song, Covalent Attachment of Anderson-Type Polyoxometalates to Single-Walled Carbon Nanotubes Gives Enhanced Performance Electrodes for Lithium Ion Batteries, *Chem. Eur. J.,* 2015, **21**, 6469.

S20.   L. B. Ni, G. Yang, C. Y. Sun, G. S. Niu, Z. Wu, C. Chen, X. X. Gong, C. Q. Zhou, G. J. Zhao, J. Gu, W. Ji, X. Huo, M. Chen, G. W. Diao, Self-assembled three-dimensional graphene/polyaniline/polyoxometalate hybrid as cathode for improved rechargeable lithium ion batteries, *Materials Today Energy,* 2017, **6**, 53.

S21.   Q. Huang, T. Wei, M. Zhang, L. Z. Dong, A. Man, Zhang, S. L. Li, W. J. Liu, J. Liu, Y. Q. Lan, A highly stable polyoxometalate-based metal– organic framework with p–p stacking for enhancing lithium ion battery performance, *J. Mater. Chem. A,* 2017, **5**, 8477.

S22.   X. Li, K. F. Zhou, Z. B. Tong, X. Y. Yang, C. Y. Chen, X. H. Shang, J. Q. Sha, Heightened Integration of POM-based Metal–Organic Frameworks with Functionalized Single-Walled Carbon Nanotubes for Superior Energy Storage, *Chem. Asian J.,* 2019, **14**, 3424.

S23.   L. J. Huang, J. Hu, Y. C. Ji, C. Streb, Y. F. Song, Pyrene-Anderson-Modified CNTs as Anode Materials for Lithium-Ion Batteries, *Chem. Eur. J.,* 2015, **21**, 18799.

S24.   J. Hu, F. F. Jia, Y. F. Song, Engineering high-performance polyoxometalate/PANI/MWNTs nanocomposite anode materials for lithium ion batteries, *Chem Eng J.,* 2017, **326**, 273.